RESEARCH BRIEF

Zenocutuzumab, a HER2xHER3 Bispecific Antibody, Is Effective Therapy for Tumors Driven by *NRG1* Gene Rearrangements

Alison M. Schram[1,2], Igor Odintsov[3,4], Madelyn Espinosa-Cotton[5], Inna Khodos[6], Whitney J. Sisso[3], Marissa S. Mattar[6], Allan J.W. Lui[3], Morana Vojnic[3,4], Sara H. Shameem[1], Thrusha Chauhan[1], Jean Torrisi[7], Jim Ford[8], Marie N. O'Connor[8], Cecile A.W. Geuijen[8], Ron C.J. Schackmann[8], Jeroen J. Lammerts van Bueren[8], Ernesto Wasserman[8], Elisa de Stanchina[6], Eileen M. O'Reilly[1,2], Marc Ladanyi[3,4], Alexander Drilon[1,2], and Romel Somwar[3,4]

ABSTRACT   *NRG1* rearrangements are recurrent oncogenic drivers in solid tumors. NRG1 binds to HER3, leading to heterodimerization with other HER/ERBB kinases, increased downstream signaling, and tumorigenesis. Targeting ERBBs, therefore, represents a therapeutic strategy for these cancers. We investigated zenocutuzumab (Zeno; MCLA-128), an antibody-dependent cellular cytotoxicity–enhanced anti-HER2xHER3 bispecific antibody, in NRG1 fusion–positive isogenic and patient-derived cell lines and xenograft models. Zeno inhibited HER3 and AKT phosphorylation, induced expression of apoptosis markers, and inhibited growth. Three patients with chemotherapy-resistant NRG1 fusion–positive metastatic cancer were treated with Zeno. Two patients with *ATP1B1–NRG1*–positive pancreatic cancer achieved rapid symptomatic, biomarker, and radiographic responses and remained on treatment for over 12 months. A patient with *CD74–NRG1*-positive non–small cell lung cancer who had progressed on six prior lines of systemic therapy, including afatinib, responded rapidly to treatment with a partial response. Targeting HER2 and HER3 simultaneously with Zeno is a novel therapeutic paradigm for patients with NRG1 fusion–positive cancers.

SIGNIFICANCE: *NRG1* rearrangements encode chimeric ligands that activate the ERBB receptor tyrosine kinase family. Here we show that targeting HER2 and HER3 simultaneously with the bispecific antibody Zeno leads to durable clinical responses in patients with *NRG1* fusion–positive cancers and is thus an effective therapeutic strategy.

[1]Department of Medicine, Memorial Sloan Kettering Cancer Center, New York, New York. [2]Weill Cornell Medical College, New York, New York. [3]Department of Pathology, Memorial Sloan Kettering Cancer Center, New York, New York. [4]Human Oncology and Pathogenesis Program, Memorial Sloan Kettering Cancer Center, New York, New York. [5]Department of Pediatrics, Memorial Sloan Kettering Cancer Center, New York, New York. [6]Anti-tumor Core Facility, Pharmacology Program, Memorial Sloan Kettering Cancer Center, New York, New York. [7]Department of Radiology, Memorial Sloan Kettering Cancer Center, New York, New York. [8]Merus N.V., Utrecht, the Netherlands.

Current address for I. Odintsov: Department of Pathology, Brigham and Women's Hospital, Boston, Massachusetts; and current address for M. Vojnic, Lenox Hill Hospital, Northwell Health, New York, New York.

Corresponding Authors: Alison M. Schram, Department of Medicine, Memorial Sloan Kettering Cancer Center, 300 East 66th Street, New York, NY 10065. Phone: 646-888-5388; E-mail: schrama@mskcc.org; and Romel Somwar, Department of Pathology, Memorial Sloan Kettering Cancer Center, 1275 York Avenue, New York, NY 10065. Phone: 212-639-2000; E-mail: somwarr@mskcc.org

INTRODUCTION

Genomic rearrangements involving the neuregulin 1 gene (*NRG1*) have been identified across several solid tumor types, including lung, breast, pancreas, ovarian, and prostate cancers (1–7). *NRG1* fusions are specifically enriched in *KRAS*-wild-type pancreatic cancer (7, 8) and *KRAS*-wild-type invasive mucinous adenocarcinoma (IMA; refs. 6, 9, 10), where they are believed to be mitogenic drivers. Chromosomal abnormalities involving *NRG1* were first identified in 1998 in breast cancer (11), and *NRG1* gene fusions were first described in 1999 in the breast cancer cell line MDA-MB-175-VII (12, 13). Chimeric NRG1 proteins contain an upstream fusion partner and retain the EGF-like domain of NRG1, which confers ligand binding and transformation (14, 15) via the ERBB family of receptor tyrosine kinases (RTK).

The ERBB RTK family consists of EGFR (ERBB1), HER2 (ERBB2), HER3 (ERBB3), and HER4 (ERBB4); these RTKs are often exploited by cancer cells to promote growth in solid tumors (16, 17). In addition to stimulation by NRG1 fusion proteins, oncogenic activation of ERBB receptors may occur directly through mutations and translocations that confer constitutive enzymatic activity (e.g., EGFR and HER2 kinase domain mutations, the EGFRvIII variant where the extracellular region of the RTK is deleted, and EGFR fusions). Such activation can also arise through gene amplification (e.g., *EGFR* and *HER2*) or protein overexpression. The identification of NRG1 chimeric ligands has led to increasing attention to constitutive ligand-induced activation and a search for therapeutics that can interfere with NRG1 action.

NRG1 binds primarily to HER3 and HER4 (18, 19), leading to heterodimerization or oligomerization with other ERBB family members. HER3 is a pseudokinase with little, if any, intrinsic enzymatic activity, making it a dependent heterodimerization partner that relies on phosphorylation from other ERBB members (20). NRG1-mediated activation of HER3 promotes asymmetric dimerization with EGFR, HER2, and HER4 (20). These partners phosphorylate HER3, forming docking sites for SH2-domain proteins, leading to activation of multiple signal transduction pathways, including the phosphoinositide 3-kinase (PI3K) pathway, culminating in cell proliferation and survival. In an experimental system in which only EGFR and HER3 are expressed, stimulation with NRG1 leads to phosphorylation of HER3 but not of EGFR; however, when only HER2 and HER3 are expressed, NRG1 induces phosphorylation of both HER2 and HER3 (21). Although the mechanism of HER2 phosphorylation in this context is unclear, it is thought that NRG1 triggers higher order oligomerization that leads to collateral HER3–HER3 interactions (21, 22). The HER2–HER3 dimers may represent the most oncogenic heterodimers of the ERBB family (23). Targeting HER2–HER3 signaling therefore represents a promising therapeutic approach for patients with NRG1 fusion–positive malignancies.

Reports of effective HER2 and/or HER3 targeting in xenograft models and in patients with IMA, cholangiocarcinoma, and pancreas cancer harboring *NRG1* rearrangements have fueled interest in exploiting these RTKs as therapy for these molecularly defined cancers (6, 7, 10, 24–27). Clinical responses to the pan-ERBB tyrosine kinase inhibitor afatinib

(10, 24) and the anti-HER3 antibody GSK2849330 have been described in case reports (24). However, no published prospective clinical trials have evaluated the efficacy of these agents in NRG1 fusion–positive cancers.

Zenocutuzumab (Zeno; MCLA-128) is a bispecific humanized immunoglobulin G1 (IgG1) containing two different Fab arms targeting the extracellular domains of HER2 and HER3 (26). The HER2-targeting arm binds to the more abundant HER2 protein on the cell surface. In addition to providing a high local concentration of the antibody, this action positions the HER3-targeting arm to block NRG1 binding to HER3 and prevent HER3 from undergoing the conformational change required for heterodimerization with HER2 and potentially with EGFR (26). This unique so-called dock (HER2 arm) and block (HER3 arm) mechanism prevents the subsequent phosphorylation of the cytoplasmic domain of HER3 and downstream oncogenic signaling (26). Further, glycoengineered modification of the IgG1 to augment affinity for Fc receptors results in enhanced antibody-dependent cellular cytotoxicity (ADCC; ref. 26). The safety and tolerability of Zeno have previously been demonstrated in a phase I study (28). Here we report the therapeutic efficacy of Zeno *in vitro* and *in vivo* in preclinical models of lung, breast, pancreas, and ovarian cancers harboring *NRG1* fusions. Moreover, we demonstrate clinical efficacy in patients with lung and pancreatic cancers driven by *NRG1* rearrangements. These results support the use of Zeno as therapy for NRG1 fusion–driven cancers of any histology in an ongoing phase I/II trial (NCT02912949).

RESULTS

Zeno Effectively Inhibits Growth of Lung and Breast Cancer Cell Lines with *NRG1* Alterations

We examined the effect of the bispecific HER2xHER3 antibody Zeno on the growth of a panel of patient-derived and isogenic cell lines expressing various *NRG1* fusions. Details of the cell lines are provided in Supplementary Fig. S1. Although the patient-derived cell lines allowed us to examine Zeno efficacy in models representing the genomic complexity of tumors, Zeno specificity could be demonstrated in the isogenic cell lines by comparing *NRG1*-rearranged cells with control cells. Growth of isogenic human bronchiolar epithelial cell lines (HBEC) expressing either a CD74–NRG1 or a VAMP2–NRG1 fusion was reduced by subnanomolar concentrations of Zeno (Fig. 1A). In contrast, growth of the isogenic control HBEC line remained largely unaffected by Zeno treatment, with maximum inhibition of approximately 25% at the highest concentration used (Fig. 1A). Comparison of the IC_{50} values for inhibition of cell growth by Zeno revealed that HBEC cells with NRG1 fusions were approximately 40,000 times more sensitive to Zeno than the parental control cells (see Supplementary Fig. S2A for IC_{50} values). Similar to the HBEC-NRG1 cell lines, growth inhibition of the lung adenocarcinoma cell line LUAD-0061AS3 (SLC3A2–NRG1; ref. 29) occurred with low nanomolar concentrations of Zeno (IC_{50} = 14.2 nmol/L; Fig. 1B and Supplementary Fig. S2A).

Given the high sensitivity of *NRG1* fusion–positive lung cancer cell lines to Zeno, we sought to examine the efficacy
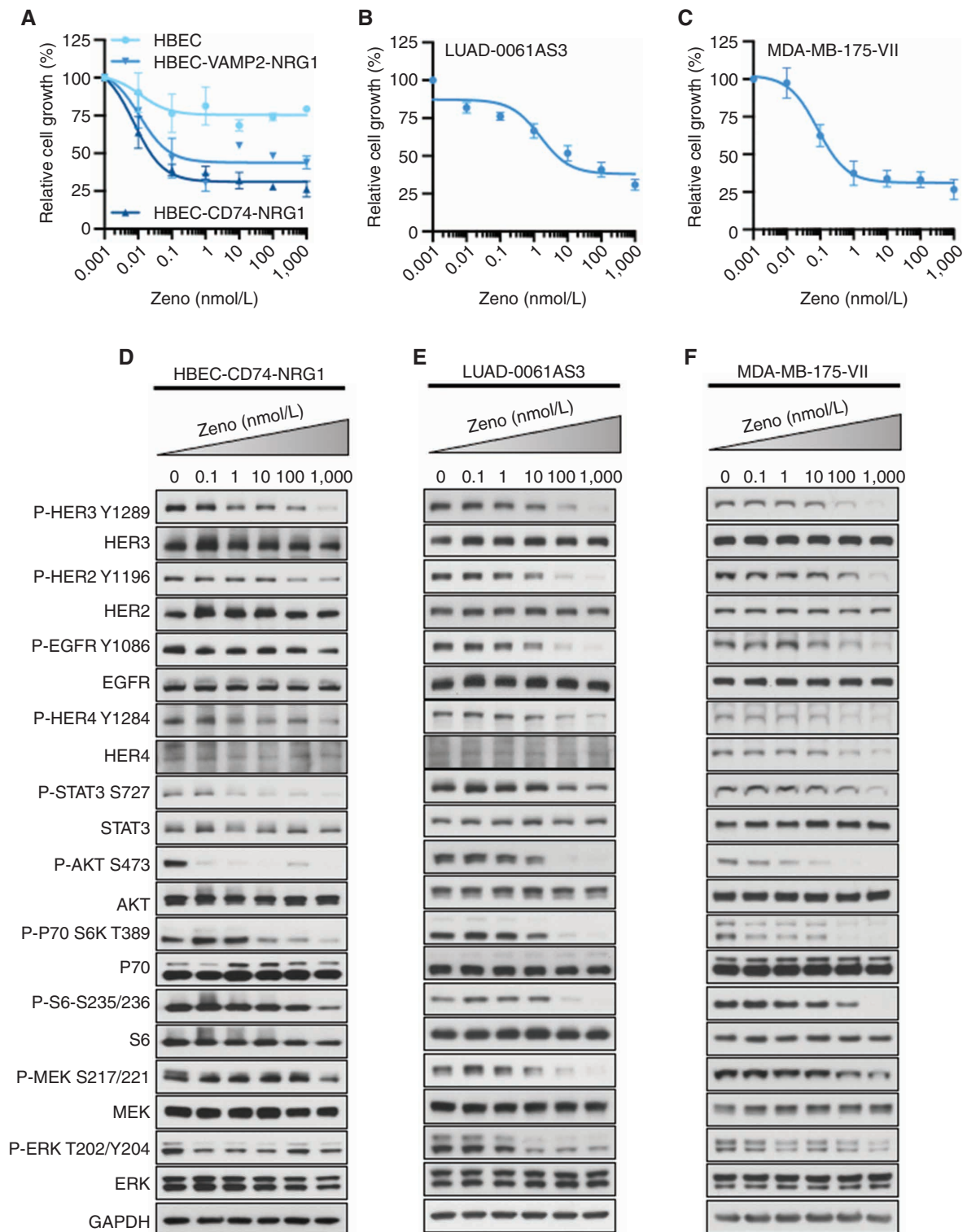
Figure 1. Zeno inhibits growth and blocks signal transduction in cell lines with *NRG1* fusions. **A–C,** Cells were treated with the indicated concentrations of Zeno for 96 hours, and then growth was determined using AlamarBlue viability dye. Values are expressed relative to the vehicle-treated control (100%). Data were analyzed by nonlinear regression to determine IC_{50} for inhibition of growth (see Supplementary Fig. S2A for IC_{50} values). Results represent the mean ± SD of three replicate determinations in one experiment. **D–F,** For Western blot analyses, cells were deprived of serum for 24 hours and then treated with the indicated concentrations of Zeno for 1.5 hours prior to preparation of whole-cell extracts and immunoblotting. Representative immunoblots are shown, with GAPDH expression used as a Western blotting loading control. At least two independent experiments were conducted.

of this antibody in breast cancer cell lines with *NRG1* fusions. We generated an isogenic pair of cell lines by ectopic expression of *DOC4* (*TENM4*)–*NRG1* cDNA in the breast cancer cell line MCF7. Expression of NRG1 fusions was confirmed by Western blotting (Supplementary Fig. S2B, left). Zeno treatment inhibited the growth of MCF7-DOC4-NRG1 cells with an IC_{50} value of 2.01 nmol/L but had a little effect on the growth of the isogenic control line MCF7-EV (IC_{50} = 4811 nmol/L; Supplementary Fig. S2C). We also examined a breast cancer cell line with an *NRG1* fusion, MDA-MB-175-VII, which expresses a complex *NRG1* fusion involving three genes (*PPP6R3–TENM4–NRG1*; 30). Of all the cell lines tested, MDA-MB-175-VII was the most sensitive to Zeno treatment, with an IC_{50} value of 0.04 nmol/L (Fig. 1C and Supplementary Fig. S2A). Finally, we examined the effect of Zeno treatment on the growth of the lung cancer cell line HCC-95, which harbors *NRG1* amplification (24). Similar to the NRG1 fusion–positive lung and breast cancer cell lines, growth of the HCC-95 cell line was also reduced by Zeno (IC_{50} = 0.15 nmol/L; Supplementary Fig. S2A and S2D). These results indicate that Zeno effectively blocks the growth of cells with *NRG1* alterations at low or subnanomolar concentrations, with comparably little effect on the growth of isogenic control cells lacking *NRG1* alterations.

## Zeno Blocks Transmission of Downstream Proliferation Signals in Lung and Breast Cancer Cell Lines

To further characterize the cellular mechanisms by which Zeno blocks the growth of *NRG1*-rearranged cell lines, we looked at the transmission of intracellular signals believed to regulate proliferation and survival in cells treated with the antibody. We found that exposure of HBEC-CD74-NRG1, LUAD-0061AS3, and MDA-MB-175-VII cells to Zeno resulted in a dose-dependent reduction in the phosphorylation of HER3, HER2, and HER4 (Fig. 1D–F). Similarly, Zeno treatment also inhibited the phosphorylation of other downstream effectors of these receptor tyrosine kinase pathways, including STAT3, AKT, p70S6K, and S6. In HBEC-CD74-NRG1 cells, 1 nmol/L Zeno led to substantial reduction in HER3 and AKT phosphorylation (Fig. 1D). EGFR phosphorylation was also reduced, mainly in LUAD-0061AS3 and MDA-MB-175-VII cells (Fig. 1E and F). Zeno treatment reduced MEK and ERK phosphorylation in LUAD-0061AS3 cells, but less so in the other two cell lines (Fig. 1D–F). Similar results were obtained in the HCC-95 cell line in which *NRG1* is amplified (Supplementary Fig. S3A). In the fusion-negative control cells, treatment with Zeno reduced phosphorylation of HER3 and HER2 at 0.1 and 10 nmol/L concentrations, respectively (Supplementary Fig. S3B and S3C). However, this did not translate to effective inhibition of downstream signaling (Supplementary Fig. S3B and S3C), as seen with the isogenic counterpart harboring CD74–NRG1 or other cell lines harboring NRG1 fusions (Fig. 1D–F). Protein expression was not altered by the 1.5-hour Zeno treatment in any of the cell lines. Taken together, these results demonstrate that 0.1 to 100 nmol/L Zeno potently inhibits the HER3–AKT–mTOR pathway in cell lines harboring *NRG1* fusions or amplification.

Zeno Treatment Induces Markers of Apoptosis and Cell-Cycle Arrest in Lung and Breast Cancer Cell Lines

To delineate the mechanism by which Zeno treatment may inhibit growth, we treated cells with *NRG1* alterations for up to 48 hours with 50 nmol/L Zeno and determined the expression of phosphorylated HER3, AKT, ERK, and S6 ribosomal protein over time, as well as that of markers of cell-cycle progression and apoptosis. In the two cell lines with *NRG1* fusions and the *NRG1*-amplified HCC-95 cell line, the phosphorylation of HER3, AKT, and S6 was almost completely shut down by 3 hours and remained suppressed throughout the 48-hour time period of the experiment (Supplementary Fig. S4A). However, the phosphorylation of ERK started to rebound by 16 hours of treatment in the LUAD-0061AS3 cell line. In MDA-MB-175-VII cells, ERK phosphorylation was already as high as basal level 3 hours after treatment (the shortest time point in these time-course studies). Prolonged treatment with Zeno did not affect the levels of total HER3, AKT, or ERK (Supplementary Fig. S4A). Increased expression of apoptosis markers (Supplementary Fig. S4A) was also observed. Enhanced levels of cleaved PARP (c-PARP) were evident as early as 3 hours after treatment began and continued to increase for the entire period of the experiment. Increased BIM expression was observed in all cell lines, with the BIM_{EL} isoform being the most responsive in the two cell lines harboring inactivating p53 mutations (LUAD-0061AS3 and HCC-95). Upregulation of PUMA in response to Zeno treatment was observed mainly in MDA-MB-175-VII cells (wild-type p53) within 3 hours of incubation, reaching a maximum by 16 hours; this high level was sustained for the rest of the 48-hour treatment time. Exposure to Zeno led to an increase in the p27 (CDKN1B) cell-cycle inhibitor and a decrease in the cyclin D1 (CCND1) protein that permits progression through the G_1 phase of the cell cycle. Levels of the p21 cell-cycle inhibitor (CDKN1A) remained unchanged in the LUAD-0061AS3 and MDA-MB-175-VII cell lines until the final time point (48 hours), when a decrease was observed (Supplementary Fig. S4A). However, in HCC-95 cells, p21 levels increased in response to Zeno treatment (Supplementary Fig. S4A). Treatment of MDA-MB-175-VII and LUAD-0061AS3 cells with Zeno resulted in a dose-dependent increase in caspase-3/7 enzymatic activity (Supplementary Fig. S4B), supporting the results from Western blotting that Zeno treatment induces apoptosis. These results indicate that Zeno is capable of sustained HER3 inhibition, blockade of the cell cycle, and induction of apoptosis.

Zeno Treatment Induces ADCC

Zeno is an IgG1 subtype antibody designed to induce enhanced ADCC through afucosylation of the Fc (26). Here, we examined Zeno for ADCC activity using peripheral blood mononuclear cells in a chromium release assay. MDA-MB-175-VII and HCC-95 cells were loaded with ^{51}Cr and then incubated with peripheral blood mononuclear cells. The amount of ^{51}Cr released by the tumor cells indicates cytotoxicity. We observed a significant increase in cytotoxicity of
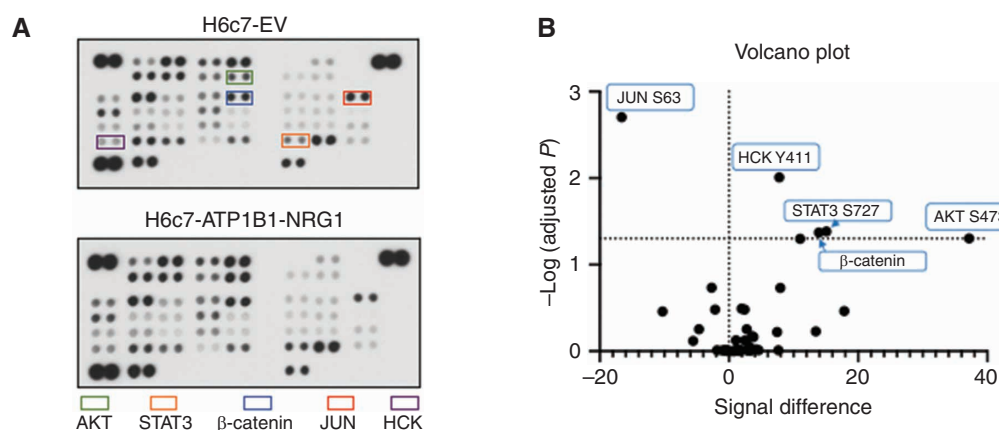
Figure 2. Zeno is effective in preclinical pancreatic cancer models. *NRG1* fusion cDNAs were expressed in the immortalized pancreatic ductal epithelial cell line H6c7. **A,** A phosphokinase array showing kinases activated in H6c7 cells expressing an empty vector (EV) or ATP1B1–NRG1 fusion. **B,** The arrays in **A** were quantitated by densitometry and a volcano plot of phosphorylation, and *P* value data are shown. Data above the horizontal dashed line represent a significantly different level of phosphorylation. Increased phosphorylation is shown to the right of the vertical dashed line and decreased phosphorylation to the left. (*continued on next page*)

the MDA-MB-175-VII and HCC-95 cells in the presence of Zeno, but not in the presence of nonspecific IgG1 molecules (Supplementary Fig. S5A and S5B). Moreover, Zeno induced a level of cytotoxicity that was higher than that caused by the anti-HER2 antibody trastuzumab. These results confirm that Zeno can induce ADCC in cells with *NRG1* fusions or amplification. Similar results have previously been shown for Zeno in SKBR-3 cells (26).

Zeno Is Effective at Blocking NRG1 Fusion–Dependent Signaling and Growth in Isogenic Pancreatic Cell Line and Xenograft Models Expressing NRG1 Fusions

We further assessed the activity of Zeno in pancreatic cells expressing NRG1 fusions. To this end, we introduced two *NRG1* fusions (*ATP1B1–NRG1* and *SLC3A2–NRG1*) into immortalized pancreatic ductal epithelial cells (H6c7). These cells can be transformed by introduction of oncogenes (8). We generated isogenic H6c7 cells stably expressing NRG1 fusions (Supplementary Fig. S2B, right) and then profiled them for activated signaling pathways using phosphoproteomic arrays (31). Expression of the ATP1B1–NRG1 fusion in H6c7 cells resulted in increased phosphorylation of several proteins, including AKT and STAT3 (Fig. 2A and B), presumably via activation of HER3. Western blotting showed that treatment of H6c7-ATP1B1-NRG1 and H6c7-SLC3A2-NRG1 cells with Zeno resulted in a dose-dependent inhibition of phosphorylation of HER3 and AKT, with complete loss of phosphorylation at a concentration of just 1 nmol/L (Fig. 2C). Some differences between the cells expressing the two fusions were noted. For example, STAT3 and HER4 phosphorylation was inhibited to a higher degree by Zeno treatment in H6c7-ATP1B1-NRG1 cells compared with H6c7-SLC3A2-NRG1 cells. As observed with the breast cancer cell line with an NRG1 fusion, phosphorylation of ERK1/2 remained largely unchanged with Zeno treatment (Fig. 2C and D). Treatment of the isogenic control H6c7-EV with Zeno decreased HER3 and HER2 phosphorylation at

100 nmol/L concentration without any substantial decrease in the other downstream signals examined (Supplementary Fig. S3C). Treatment of animals bearing H6c7-SLC3A2-NRG1 xenograft tumors with Zeno (25 mg/kg, once weekly) slowed tumor growth significantly (Supplementary Fig. S6A and S6B) without affecting animal weight (Supplementary Fig. S6C). We next examined the efficacy of Zeno in a pancreatic adenocarcinoma patient-derived xenograft (PDX) model harboring an *APP–NRG1* fusion (CTG-0943). Treatment of mice bearing CTG-0943 PDX tumors with 2.5, 8, or 25 mg/kg Zeno once weekly resulted in a dose-dependent reduction in tumor growth (Fig. 2D). Area under the curve (AUC) analysis showed that each of the three Zeno doses caused a significant reduction in tumor volume (Fig. 2E), with the 25 mg/kg once weekly dose being the most effective. Nine of the 10 tumors in the 25 mg/kg once weekly group shrank by >50%, resulting in a 63% ± 17% decrease in tumor volume (Fig. 2F). These results support the data obtained with the H6c7-SLC3A2-NRG1 xenograft model, showing that Zeno therapy could be effective in pancreatic cancers driven by *NRG1* fusions.

Zeno Is Effective at Blocking Growth of Lung and Ovarian Cancer PDX Models at Clinically Relevant Doses

The data above indicate that Zeno effectively inhibits growth and signal transduction in cell lines with *NRG1* alterations. We further analyzed the ability of Zeno to block the growth of NRG1 fusion–positive PDX tumors from lung cancers (*CD74–NRG1* and *SLC3A2–NRG1*) and from a high-grade serous ovarian cancer (HGSOC; *CLU–NRG1*). Animals bearing established PDX tumors were treated once per week with Zeno (2.5, 8, or 25 mg/kg). Growth of the ST3204 model (lung cancer, *CD74–NRG1* fusion) was blocked at all doses of Zeno tested (Fig. 3A, left). AUC analysis showed that all doses of Zeno caused a statistically significant reduction of growth, including tumor regression (Fig. 3A, middle). There was no difference between the three Zeno-treated groups, and tumor shrinkage was evident in all groups by the

C

D CTG-0943, *APP–NRG1* pancreatic cancer PDX

E

F
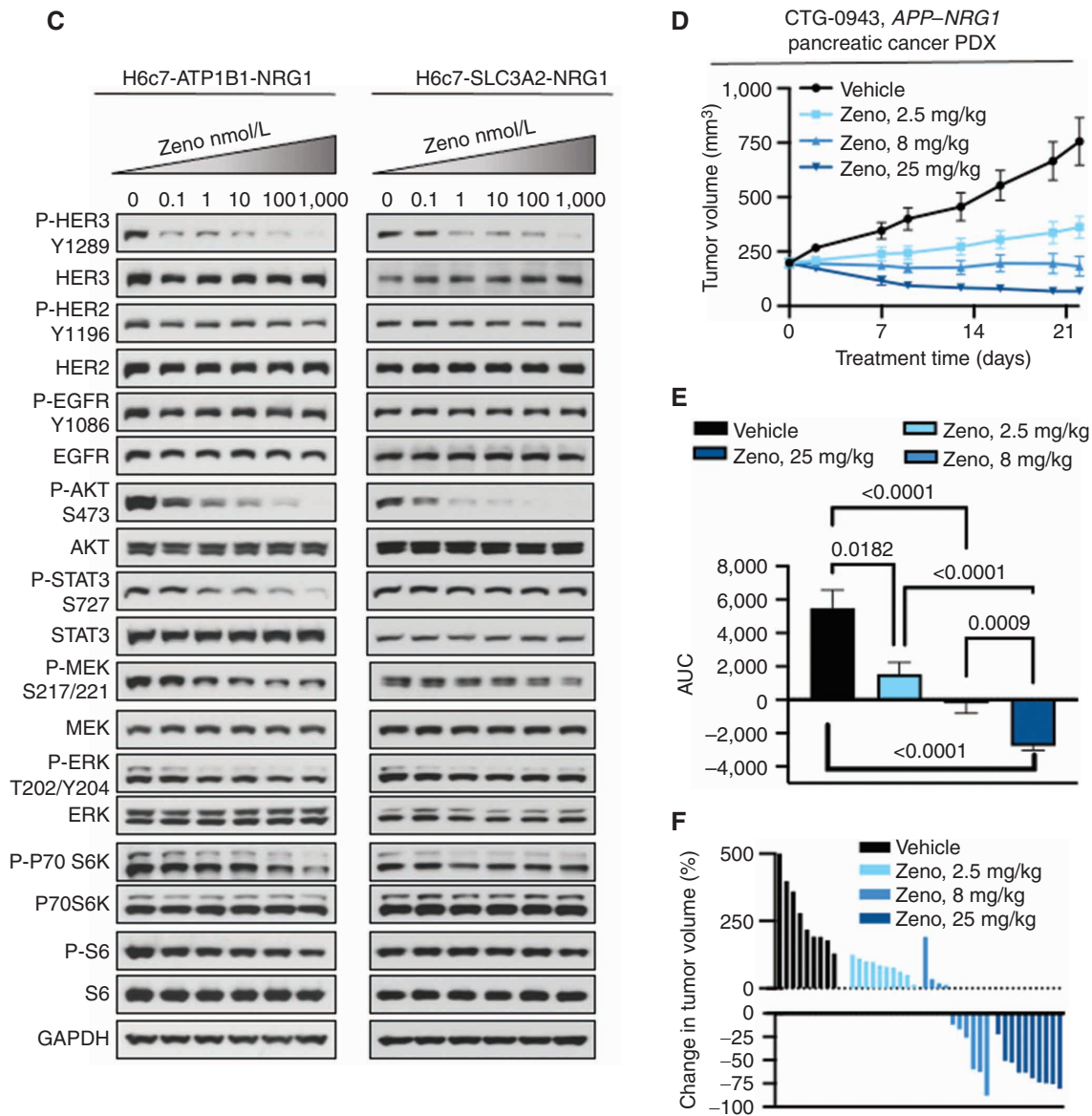
Figure 2. *(Continued)* **C,** H6c7-ATP1B1-NRG1 and H6c7-SLC3A2-NRG1 cells were serum-starved for 24 hours and then treated with Zeno for 1.5 hours. Whole-cell extracts were then prepared and subjected to Western blotting. Representative immunoblots are shown, with GAPDH expression used as a Western blotting loading control. At least two independent experiments were conducted. **D–F,** A pancreatic adenocarcinoma PDX model (CTG-0943) was treated with the indicated dose of Zeno weekly. There were 10 animals per group. Tumor volume over time is shown in **D**. AUC analysis of tumor volumes is shown in **E**. The percentage change in the volume of individual tumors is shown in **F**.

third day after treatment initiation. All Zeno-treated ST3204 tumors shrank by 50% to 100%, with the exception of one tumor in the 8 mg/kg group, which shrank initially by >50% but started to regrow toward the end of the study (Fig. 3A, right). There was one complete response (100% shrinkage). Treatment of a second lung cancer PDX model with a CD74–NRG1 fusion (ST2891) resulted in a dose-dependent reduction in tumor volume (Supplementary Fig. S6D). AUC analysis showed the reduction in tumor growth was statistically significant for the 8 and 25 mg/kg groups compared with vehicle-treated tumors (Supplementary Fig. S6E). Two ST2891 tumors (one in the 8 mg/kg group and one in the

25 mg/kg group) shrank by 37% by the end of the study (Supplementary Fig. S6F).

Administration of Zeno to mice implanted with LUAD-0061AS3 PDX tumors resulted in a dose-dependent reduction in tumor growth (Fig. 3B, left), and AUC analysis showed that tumor growth in all Zeno-treated groups was significantly lower than for vehicle-treated tumors (Fig. 3B, middle). In this model, tumor shrinkage was observed in the 8 and 25 mg/kg groups (Fig. 3B, right), and, as also observed in the ST3204 model, this was evident by the fourth day of treatment. Administration of Zeno was continued for 25 days after sacrifice of the animals in the vehicle arm (due to tumor
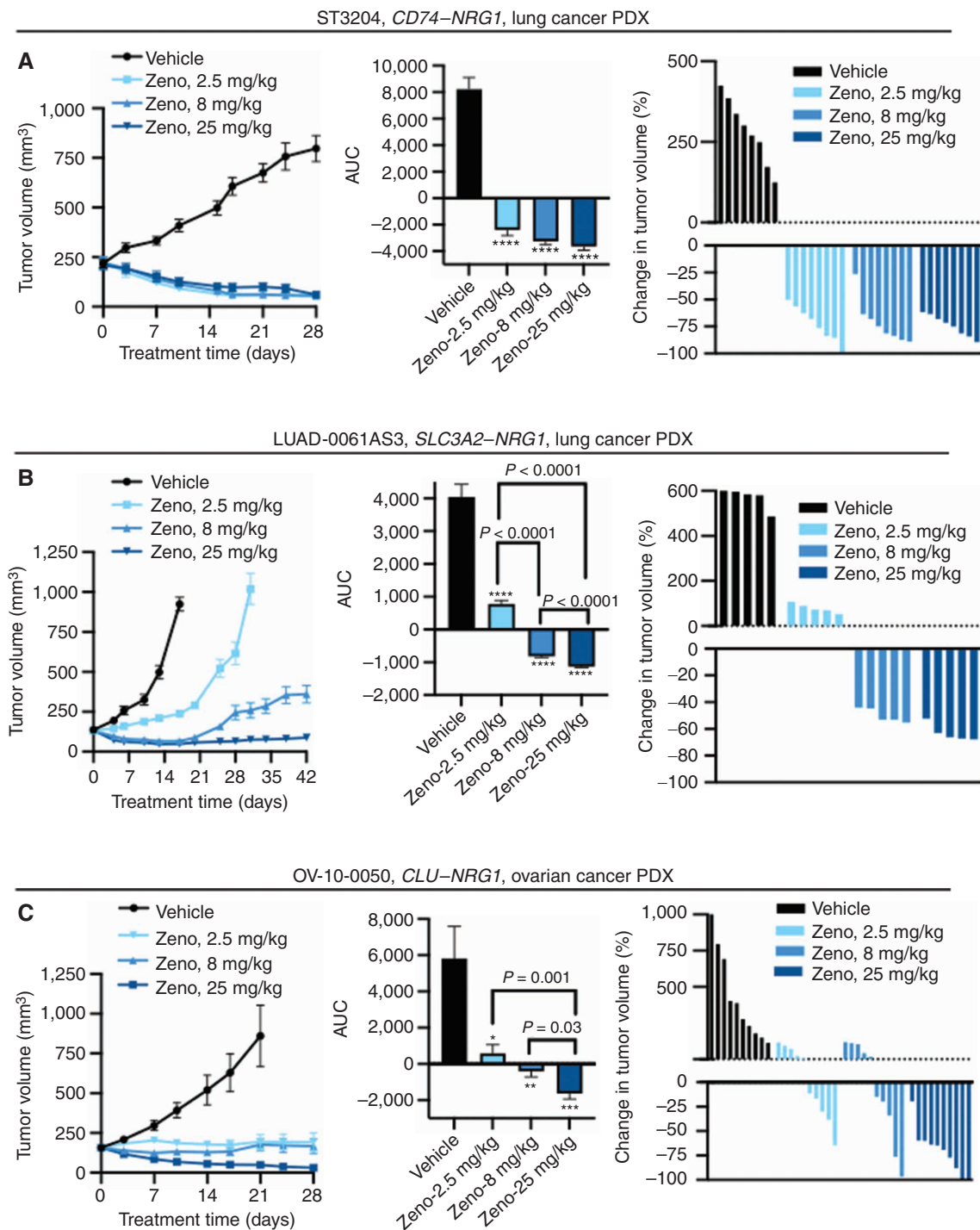
Figure 3. Zeno induces tumor regression in PDX models of *NRG1*-rearranged cancers. Mice bearing PDX tumors were treated with the indicated doses of Zeno once weekly. The tumor volume (left), AUC (middle), and change in volume of individual tumors at the time representative of the AUC analysis (right) are shown for each model. **A,** ST3204 PDX model (lung cancer; eight mice per group). AUC analysis was performed for the time period ending on day 28. Tumor growth in Zeno-treated animals was significantly lower than that in vehicle-treated animals as measured by AUC (****, $P < 0.0001$), with no significant difference between the AUC values of the Zeno-treated groups ($P > 0.05$). **B,** LUAD-0061AS3 PDX model (lung cancer; five mice per group). AUC analysis was performed for the time period ending on day 17. ****, $P < 0.0001$ compared with the vehicle-treated group. **C,** OV-10-0050 PDX model (HGSOC; 10 mice per group). AUC analysis was performed for the time period ending on day 21. *, $P = 0.03$; **, $P = 0.006$; ***, $P = 0006$ compared with the vehicle-treated group. Results in all left and middle plots represent mean ± SEM. Administration of Zeno had no adverse effect on animal weight during the course of treatment (Supplementary Fig. S4).

size) to evaluate durability of the response to Zeno (Fig. 3B, right). Tumors in the 25 mg/kg group, a dose that results in similar steady-state serum concentrations as attained in the current human patient treatment regimen (750 mg every 2 weeks), remained significantly smaller than the average starting size [size before treatment (mean ± SEM): 133.45 ± 2.36 mm³; size at study end: 88.85 ± 5.78 mm³]. The best response in the two groups that showed tumor regression was 50% and 64% tumor shrinkage, respectively, for the 8 mg/kg and 25 mg/kg groups. Western blotting analysis of tumors extracted after Zeno treatment showed substantial reduction in HER and p70S6K phosphorylation, as well as downregulation of cyclin D1 and induced expression of c-PARP (Supplementary Fig. S6G and S6H). These results suggest that Zeno treatment likely caused tumor regression by inhibiting the cell cycle and inducing apoptosis.

Expanding the histologic groups of cancer with *NRG1* fusions that may benefit from Zeno therapy, we examined the efficacy of the antibody in a PDX model derived from HGSOC. This PDX model (OV-10-0050) expresses a *CLU–NRG1* fusion and has previously been shown to respond to anti-HER2xHER3 therapy (24, 26, 27). Treatment of mice implanted with OV-10-0050 PDX tumors resulted in a dose-dependent reduction in growth (Fig. 3C, left). AUC analysis showed that tumor growth in all Zeno-treated groups was significantly lower than for vehicle-treated tumors (Fig. 3C, middle). Growth was reduced by 70.5% ± 7.4% in the 25 mg/kg group, and nine of 10 tumors in this group shrank by ≥60%, with two complete regressions (Fig. 3C, right). Zeno treatment did not cause any reduction in animal weight in any of the studies (Supplementary Figs. S6C and S7A–S7E) or any sign of ill health.

Clinical Proof of Efficacy in NRG1 Fusion–Positive Patients

Three patients with chemotherapy-resistant metastatic cancer were found to have *NRG1* fusion–positive tumors on genomic sequencing performed as part of routine care at Memorial Sloan Kettering Cancer Center (MSKCC). Zeno's promising activity in NRG1 fusion–positive preclinical models, its previously established favorable toxicity profile in patients with HER2⁺ breast and gastric cancer, and the absence of available clinical trials for this population at the time led us to initiate Zeno treatment on single-patient protocols (26, 28). All three patients experienced dramatic clinical and radiographic responses.

The first patient was a 50-year-old man who presented with stage IIB (pT3N1cM0) pancreatic ductal adenocarci-

noma (PDAC). He underwent a pylorus-sparing pancreaticoduodenectomy (Fig. 4A). DNA profiling of the tumor with the MSK-Integrated Mutation Profiling of Actionable Cancer Targets (MSK-IMPACT; ref. 32) platform revealed no *KRAS* mutation or other potential oncogenic driver (Supplementary Table S1). A postoperative CT scan showed no evidence of cancer, and he was treated with adjuvant chemotherapy consisting of gemcitabine and capecitabine. Unfortunately, his first scan 4 months into treatment demonstrated new liver metastases. Chemotherapy was changed to FOLFIRINOX (5-fluorouracil, leucovorin, irinotecan, and oxaliplatin). FOLFIRINOX was poorly tolerated, as the patient experienced side effects including hypotension, hypertension, nausea, vomiting, and neuropathy. Thus, adjustments to treatment including dose reductions, split dosing, and omission of either irinotecan and/or oxaliplatin were made. He continued on chemotherapy for 9 months, during which time his CA 19-9 (a tumor marker) levels continued to rise and CT scans revealed enlarging liver metastases. To further evaluate his tumor's genomics in the absence of a known *KRAS* mutation, RNA sequencing was performed on tissue from his primary resection using the MSK solid tumor fusion panel (33). This assay identified an in-frame fusion of *ATP1B1* exon 2 with *NRG1* exon 2. Given the *NRG1* gene fusion in his tumor, the lack of approved targeted therapy or appropriate clinical trials at that time for patients with this alteration, and the favorable activity foreseen with Zeno in this study, the patient then started Zeno on a single-patient protocol. Zeno was administered as an intravenous (i.v.) infusion, 750 mg every 2 weeks. Within weeks of treatment initiation, he achieved a clinical and pharmacodynamic response to therapy with improvement in his fatigue and anorexia, and a reduction in CA 19-9 levels from 262 to 56 U/mL. Imaging at 8 weeks demonstrated a partial response (−44%) according to the Response Evaluation Criteria in Solid Tumors (RECIST) guidelines (version 1.1) and a complete response by PET response criteria (Fig. 4B; refs. 34, 35). His partial response continued with further tumor shrinkage to −82% before ultimately progressing 14 months into treatment. Cell-free DNA (cfDNA) sequenced at the time of progression using a targeted next-generation sequencing (NGS) panel, MSK-ACCESS (36), demonstrated an emergent PTEN mutation (R233*). He continued on treatment for an additional five months for continued clinical benefit before being taken off therapy.

The second patient was a 34-year-old man who presented with PDAC metastatic to the liver. DNA-based sequencing determined that his tumor was *KRAS* wild-type (Supplementary Table S1). He was treated with FOLFIRINOX for 14 months (Fig. 4C). Oxaliplatin was discontinued after cycle

Figure 4. Clinical responses to Zeno. **A,** Clinical course of a 50-year-old man with *ATP1B1–NRG1* fusion–positive PDAC treated with Zeno (top), including tumor volume and CA 19-9 levels during Zeno treatment (bottom). Best overall response is indicated for each therapy, including progressive clinical disease (PD) and partial response (PR) as defined by RECIST v1.1. **B,** Representative tumor imaging of this patient's liver metastases at baseline and 8 weeks into treatment with Zeno. **C,** Clinical course of a 34-year-old man with *ATP1B1–NRG1* fusion–positive PDAC treated with Zeno (top), including tumor volume and CA 19-9 levels during Zeno treatment (bottom). Best overall response is indicated for Zeno [stable disease (SD) as defined by RECIST v1.1]. **D,** Representative tumor imaging from this patient showing a CT scan of the pancreas performed at baseline and 7 weeks into treatment with Zeno, and a PET scan 10 weeks into treatment showing non–FDG-avid liver metastases (no baseline available). **E,** Clinical course of a 52-year-old man with *CD74–NRG1* fusion–positive NSCLC treated with Zeno after six prior lines of systemic therapy and multiple courses of radiation. Best overall response is labeled for each therapy, including clinical PD/SD and PR as defined by RECIST v1.1. **F,** Tumor shrinkage in this patient depicted graphically (left) and by representative tumor imaging (right) performed at baseline and 16 weeks into Zeno treatment. cape, capecitabine; carbo, carboplatin; gem, gemcitabine; LL, left lower; LUL, left upper lobe; MDS-EB1, myelodysplastic syndrome with excess blasts-1; pem, pemetrexed; PORT, postoperative radiotherapy; SRS, stereotactic radiosurgery; vin, vinorelbine.

American Association for Cancer Research
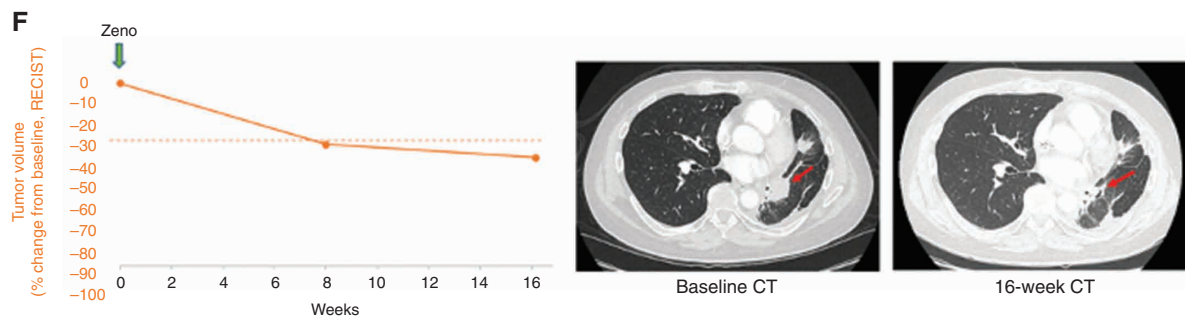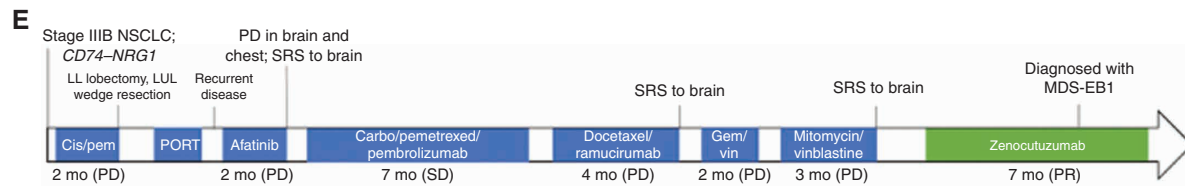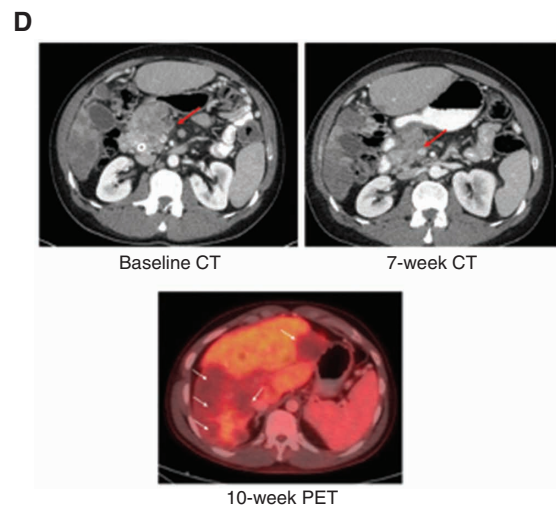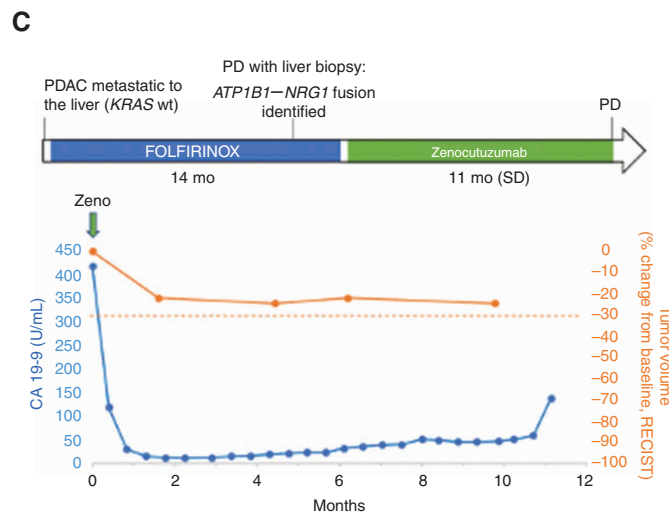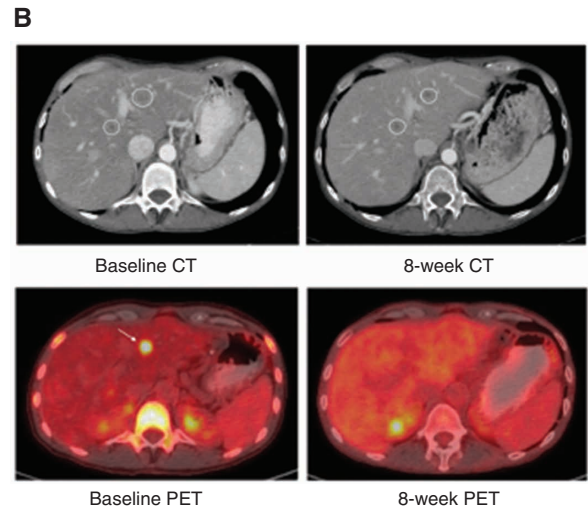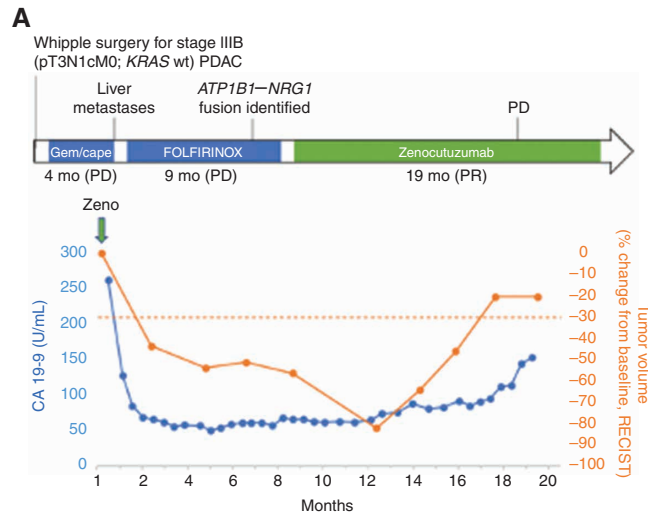
11 due to neuropathy. He initially responded well to therapy, but 10 months into treatment, when his chemotherapy was delayed for travel, he developed disease progression requiring an endoscopic retrograde cholangiopancreatography (ERCP) with biliary stent placement. A liver biopsy was performed, and RNA sequencing identified an in-frame fusion of *ATP1B1* exon 2 with *NRG1* exon 2. He was initiated on Zeno 750 mg i.v. every 2 weeks. He experienced rapid resolution of his tumor-associated abdominal pain and normalization of CA 19-9 levels (418–11 U/mL). Imaging at 6 weeks showed tumor reduction of 22% that further decreased on subsequent imaging (−25%; Fig. 4D). He continued on treatment for 11 months before developing clinical disease progression with worsening abdominal and back pain. Profiling of cfDNA using MSK-ACCESS at the time of progression showed new CDKN2A H83D and TP53 G266* mutations.

The third patient was a 52-year-old man diagnosed with stage IIIB non–small cell lung cancer (NSCLC), mixed mucinous and nonmucinous adenocarcinoma. MSK-IMPACT profiling detected a fusion between *CD74* exon 7 and *NRG1* exon 6, and no other driver alterations in *EGFR, KRAS, ALK, ROS1, RET, BRAF, HER2, METex14,* or *NTRK* (Supplementary Table S1). He was treated with neoadjuvant cisplatin and pemetrexed, followed by a left lower lobectomy, left upper lobe wedge resection, mediastinal and regional lymphadenectomy, and postoperative radiation (Fig. 4E). The first posttreatment CT scan showed new lung metastases. He was initiated on afatinib to target the *NRG1* fusion but developed rapid clinical and radiologic disease progression including new brain and lung metastases. He was subsequently treated with carboplatin, pemetrexed, and pembrolizumab for four cycles, followed by pemetrexed/pembrolizumab maintenance with stable disease lasting 5 months before radiographic progression. He went on to receive three additional lines of systemic therapy and two rounds of stereotactic radiosurgery (SRS) to the brain. Unfortunately, his disease was chemorefractory, and he progressed through each line of chemotherapy. In an attempt to target the *NRG1* fusion identified in his tumor, he was started on Zeno under a single-patient protocol, 750 mg i.v. every 2 weeks. He responded rapidly to treatment, with scans showing a partial response (−33%) by RECIST v1.1 at 8 weeks and tumor shrinkage in the brain (Fig. 4F). His response further deepened at 4 months (−41%), with improvement in his chronic dizziness. Five months into treatment, he became pancytopenic. A bone marrow biopsy confirmed myelodysplastic syndrome (MDS) with excess blasts (MDS-EB1), which was believed to be related to his prior chemotherapy and radiation treatments and unrelated to Zeno. In this setting, Zeno was held, and he developed worsening MDS and progressive lung cancer. Zeno was briefly restarted given the prior clinical benefit; however, he experienced a rapid clinical decline with refractory cytopenias and development of hemorrhagic metastases. He was placed in hospice care and died shortly thereafter.

DISCUSSION

Solid tumors driven by *NRG1* fusions comprise a molecularly defined subset of cancer for which there is no approved therapy targeting the driver genomic alteration. Here we examined the efficacy of targeting HER3, the predominant receptor for oncogenic NRG1 fusions, through a unique "dock and block" mechanism using Zeno, a HER2xHER3 bispecific antibody (26). Treatment of NRG1 fusion–positive cell lines and/or PDX models generated from lung, breast, ovarian, and pancreatic cancers with Zeno at or below clinically relevant doses resulted in reduced cell growth, induction of apoptosis, and tumor shrinkage in some PDX models. Mechanistic studies demonstrated that Zeno potently decreased phosphorylation of HER2, HER3, EGFR, and HER4 and reduced transmission of NRG1 fusion–dependent signaling via growth and survival pathways such as AKT, mTOR, and STAT. Notably, the MEK–ERK pathway was less responsive to Zeno treatment in three of the five cell lines with NRG1 fusions that we tested. Suppression of NRG1 fusion–dependent signaling resulted in loss of expression of the cell-cycle activator cyclin D1 and increased expression of cell-cycle inhibitors (P21 and P27) in addition to increased expression of the proapoptotic proteins BIM, c-PARP, and PUMA. Taken together, these results demonstrate that Zeno inhibits the growth of tumors driven by *NRG1* rearrangements by blocking downstream signaling, reducing entry into the cell cycle, and inducing cell death. The efficacy of Zeno in NRG1 fusion—positive cell lines but not isogenic nonfusion counterparts suggests that NRG1 alterations confer oncogene addiction. To our knowledge, NRG1 is the first oncogenic genomically altered receptor ligand, and cancers with NRG1 fusions are the first malignancies arising from fusion proteins to be effectively targeted with antibody therapy.

Although Zeno treatment lowered HER2 and HER3 phosphorylation in isogenic control HBEC and H6c7 cell lines, this did not translate into substantial inhibition of downstream signaling. This contrasts with the isogenic counterparts expressing NRG1 fusions. These results further show that expression of NRG1 fusions co-opt downstream growth and survival pathways to drive tumorigenesis. Although we observed differential sensitivity of cell lines to Zeno, we were unable to see any relationship between the tissue of origin of the cell lines or the fusion partner and sensitivity to Zeno. Similarly, we noted varying sensitivity of PDX models to Zeno. The LUAD-0061AS3 PDX model with an *SLC3A2–NRG1* fusion and the ST3204 model with a *CD74–NRG1* fusion responded very well to Zeno therapy, with all tumors shrinking >50% with the 25 mg/kg once weekly dose. However, data obtained with the ST2891 PDX model, which also harbors a *CD74–NRG1* fusion, showed that only one tumor in the group showed tumor regression. The limited number of models and fusions prevents us from making conclusions as to whether any histology or tumor with a particular fusion partner is more likely to respond to Zeno.

Given the mechanistic and preclinical data, Zeno was tested in three patients with chemotherapy-resistant NRG1 fusion–positive metastatic cancer prior to the availability of a clinical trial, all of whom experienced unequivocal clinical benefit. Two patients with *ATP1B1–NRG1* fusion–positive pancreatic cancer experienced tumor shrinkage, resolution of disease-related symptoms, and profound improvement in quality of life. They continued on therapy with minimal toxicity for 19 and 11 months. This is especially remarkable given the unmet

need in pancreatic cancer, with more than half of patients dying within a year of treatment initiation (37). There are currently no approved therapies after first- and second-line chemotherapy, and patients are typically treated with supportive care or enrolled in a clinical trial. Targeted therapy trials for pancreatic cancer have previously focused on the use of monoclonal antibodies and kinase inhibitors targeting primarily EGFR, VEGF, or KRAS without significant benefit, even when combined with systemic chemotherapy (38, 39). More recently, the observation that 4% to 7% of patients with pancreatic cancer harbor germline *BRCA* (g*BRCA*) mutations has led to clinical trials targeting DNA repair pathways and the approval of olaparib as maintenance therapy after chemotherapy in this population (40). Although g*BRCA* mutations occur in a minority of patients with pancreatic cancer, the validation of a genomic biomarker in this population is likely to increase the rate of both germline and somatic testing, thus identifying patients with *NRG1* fusions. Importantly, *NRG1* rearrangements are often not detected by DNA-based sequencing techniques due to the large introns in *NRG1* that are not typically included in targeted panels or whole-exome sequencing. RNA-based sequencing is a superior method for identifying these alterations and should be performed in patients with *KRAS* wild-type pancreatic cancer to look more comprehensively for *NRG1* fusions.

The third patient, a man with otherwise driver-negative NSCLC, experienced a partial response and disease control in the brain for several months before unfortunately developing unrelated clinical decompensation. Despite having rapidly progressed through six lines of prior systemic therapy, including afatinib, he had brisk tumor shrinkage on Zeno. Interestingly, his lack of response to prior therapy may reflect a more universal tendency for *NRG1* fusion–positive NSCLC to have poor prognostic features and respond poorly to standard chemoimmunotherapy (41). Moreover, *NRG1* rearrangements are typically mutually exclusive with alterations in other drivers in lung cancer such as *EGFR*, *KRAS*, *ALK*, *ROS1*, *RET*, and *NTRK*, further limiting treatment options (1). Therefore, although many therapies exist for lung cancer, patients with tumors driven by *NRG1* fusions are still in desperate need of better therapy.

Zeno is an ADCC-enhanced anti-HER2xHER3 bispecific antibody that "docks" on HER2 to optimally position the antibody to bind HER3 and subsequently "block" NRG1 from interacting with HER3, effectively preventing HER2:HER3 heterodimerization and downstream signaling (26). This unique mechanism of action seems optimally suited for treating patients with NRG1 fusion–positive cancer. Although clinical responses to other HER2- and/or HER3-targeted therapies have been reported in patients harboring NRG1 fusions, it is not possible to determine response rates or compare therapies due to the anecdotal nature of these reports, the general bias toward publishing positive results, and the heterogeneity of the methods used to assess clinical benefit outside of a clinical trial setting. Similarly, a notable drawback of our report is the small number of patients described, limited by the number of patients treated on single-patient protocols at MSK. We expect to better understand the efficacy of Zeno when results from a larger multi-institutional clinical trial are published.

We previously reported a durable partial response lasting 19 months in a patient with NSCLC treated with the anti-HER3 antibody therapy GSK2849330 (24). In a published report summarizing 19 cases treated with afatinib, seven cases showed partial responses lasting from 3 to 12 months and three cases lasting 18 to 27 months (25). Five cases showed stable or progressive disease. Notably, the toxicity with afatinib is significant and may be particularly challenging in the *NRG1* fusion–positive population. In a phase III study of afatinib versus cisplatin in *EGFR*-mutant lung cancer, more than half of patients (52%) required dose reductions for toxicity, and 95% had treatment-related diarrhea, including 14% with grade 3 diarrhea (42). The high likelihood for drug-induced diarrhea is especially concerning when treating patients with pancreatic cancer who often have some degree of pancreatic insufficiency leading to chronic diarrhea. This is in stark contrast with Zeno, which is well tolerated, with treatment-related diarrhea—all grade 1 or 2—seen in only 20% of patients (the most common related adverse event; ref. 41). As a comparison, 66% of patients treated with GSK2849330 in a phase I trial had treatment-related diarrhea (43).

There has been no published direct comparison of Zeno with other potential anti-HER therapies such as afatinib, seribantumab, or GSK2849330 in NRG1 fusion–positive PDX models. Comparing previously published studies in the LUAD-0061AS3 PDX model (29) and the current study, Zeno (25 mg/kg once weekly) was more effective than GSK2849330 (25 mg/kg twice a week) at causing tumor regression. Seribantumab was as effective as Zeno at inhibiting the growth of LUAD-0061AS3 PDX tumors. In the OV-10-0050 ovarian cancer model, GSK2849330 and seribantumab (all PDX tumors shrank by 100%) were more effective than Zeno at different doses used (24, 27). However, caution should be exercised in interpreting these preclinical data, as none of these potential therapeutic agents were compared in the same study.

In summary, the data presented in this study underscore the treatment potential for Zeno, an anti-HER2xHER3 bispecific antibody, as a new treatment specifically targeting *NRG1* fusion–positive cancers. Zeno binds to and blocks HER3 from interacting with NRG1 or the NRG1 fusion protein. This inhibition leads to potent efficacy in preclinical models and durable responses in patients who have few, if any, therapeutic options. Zeno is a promising therapeutic option in development for patients with NRG1 fusion–positive cancers. Based on this proof of concept, a global, multicenter phase I/II clinical trial for *NRG1* fusion–positive cancers has been initiated (eNRGy trial, NCT02912949).

METHODS

A list of antibodies used in this study is provided in Supplementary Table S2.

Cell Lines and PDX Models

The breast cancer epithelial cell lines MDA-MB-175-VII (cat. #HTB-25, RRID: CVCL_1400) and MCF-7 (cat. #HTB-22, RRID: CVCL_0031) were obtained from the ATCC. MDA-MB-175-VII cells express a *DOC4–NRG1* fusion (12, 24). MCF-7 cells were derived from a pleural effusion isolated from a patient with breast cancer and are estrogen receptor–positive (44). This cell line has been profiled by the Broad Institute DepMap program and does not have any *NRG1* rearrangement (45).

Human bronchial epithelial cells were immortalized by overexpression of CDK4 and TERT (HBEC-3KT cell line) and were obtained from Dr. John Minna (UT Southwestern, Dallas, TX; ref. 46). A p53 C-terminal mutant was introduced into HBEC-3KT (HBECp53) as described previously (47) and a CD74–NRG1 or VAMP2–NRG1 (custom synthesized by GeneCopoeia) fusion was expressed in these cells by lentiviral-mediated transduction of the cDNAs. Stable cell lines were selected with 200 μg/mL hygromycin. The immortalized pancreatic ductal epithelial cell line H6c7 (CVCL_0P38; ref. 48) was purchased from Kerafast. The *DOC4–NRG1, ATP1B1–NRG1,* and *SLC3A2–NRG1* fusions were amplified by PCR from MDA-MB-175-VII cells, a pancreatic adenocarcinoma sample, and LUAD-0061AS3 cells, respectively, and then cloned into the retroviral pCX4 vector. Cells were transduced with PCX4-empty plasmid or PCX4–NRG1 fusion plasmids. Cells expressing the empty plasmid or fusion were selected using 750 μg/mL bleomycin. HCC-95 cells were obtained from Dr. William Lockwood (BC Cancer Center, Vancouver, BC, Canada, RRID: CVCL_5137), and these cells were found to have *NRG1* amplification by whole-exome sequencing (24). The LUAD-0061AS3 PDX model was generated from a sample obtained from a patient with *SLC3A2–NRG1* fusion–driven lung cancer. The patient was progressing on afatinib (40 mg/day) at the time of collection of the sample used to generate the model as described previously (29). The LUAD-0061AS3 cell line was generated from LUAD-0061AS3 PDX tumor tissue obtained after seven serial passages (29). Cell lines were tested for *Mycoplasma* every 3 to 6 months (MycoAlert Kit, Lonza), with the most recent testing conducted 3 months prior to completion of the experiments in this study. Authenticated cell lines purchased from ATCC 1 year prior to the studies were expanded, and stocks were frozen. A new vial of cells was thawed and used for 10 to 15 passages (every 2 months), and the known oncogene was verified by RT-PCR each time. The identity of models that were created in our laboratory was confirmed by MSK-IMPACT profiling, and this was routinely confirmed by testing for the known oncogene fusion. The ST3204 and ST2891 lung cancer PDX models were genomically characterized by RNA sequencing, and the *CD74-NRG1* fusion was confirmed by XenoStart. The CTG-0943 pancreatic adenocarcinoma PDX model was genomically characterized by RNA sequencing, and the *APP–NRG1* fusion was confirmed by Champions Oncology. The OV-10-0050 PDX model was characterized by RNA sequencing, and the *CLU–NRG1* fusion was confirmed by PCR (27).

Growth and Propagation of Cell Lines

The MDA-MB-175-VII cell line was maintained in DMEM:Ham's F12 (1:1) medium supplemented with 20% FBS. For experiments, MDA-MB-175-VII cells were plated and grown in DMEM:Ham's F12 medium containing 10% FBS. MCF-7 cells were grown in DMEM supplemented with 10% FBS. HBECp53 cells were grown in KSM supplemented with bovine pituitary extract and EGF. Isogenic HBECp53 cell lines expressing NRG1 fusions were grown in DMEM:Ham's F12 (1:1) medium supplemented with 10% FBS. HCC-95 cells were grown in RPMI 1640 supplemented with 10% FBS. All growth media were supplemented with 1% antibiotic (penicillin/streptomycin mixture). Cells were subcultured using trypsin (0.25%)/EDTA (1 mmol/L) when stock flasks reached 75% confluency and replated at a 1:3 dilution. Cells were kept in a humidified incubator infused with 5% CO_2 and maintained at 37°C.

Growth and Apoptosis Assays

For dose–response studies, cells were plated at a density of 3,500 cells in white, clear-bottom 96-well plates in a volume of 100 μL complete growth medium. Twenty-four hours later, the growth media were replaced with 180 μL serum-free media as described previously and 20 μL inhibitors added at 10× concentration (to achieve 1× concentration) in a final volume of 200 μL. After 96 hours incubation, 20 μL AlamarBlue cell viability reagent was added to achieve a final

concentration of 10%. AlamarBlue is a cell-permeable pH-sensitive dye that is reduced when it enters the mitochondria and emits fluorescence at a different wavelength. Fluorescence was measured (Ex: 530 nm, Em: 585 nm) using a Molecular Dynamics Spectramax M2 fluorescence plate reader. In each experiment, background fluorescence was determined in cells treated with 1 μmol/L of the 20S proteasome inhibitor carfilzomib, which is toxic to most cells at high concentrations, and this background was subtracted from all values. There were three to four replicates of each condition. Relative IC_{50} and 95% confidence interval values were determined by nonlinear regression analysis using GraphPad Prism 8 software using either a variable slope model or, in cases where inhibition was only partial, a three-parameter fit. The curve fitting resulted in $R^2 > 0.8$ for the data sets. Each condition was assayed in triplicate in at least two independent experiments. Caspase-3/7 enzymatic activity was measured using a fluorescence-based assay as previously described (27).

Efficacy Studies in Animals

Animal care and experiments were conducted in accordance with a protocol approved by the MSKCC Institutional Animal Care and Use Committee and Research Animal Resource Center and in accordance with Institutional Animal Care and Use Committee–approved protocols at Wuxi AppTec, XenoSTART, and Champions Oncology. Crushed PDX tumor samples were mixed with matrigel (50%) and injected into the subcutaneous flank of 6- to 12-week-old female NSG (LUAD-0061AS3), BALB/c nude (OV-10-0050), or athymic nude (ST2891, ST3204, and CTG-0953) mice. When tumors reached approximately 125 to 250 mm³, mice were randomized to groups of 5 to 10 and treatment commenced. Zeno was administered in phosphate-buffered saline by injection into the peritoneal cavity once per week. Mice were observed daily throughout the treatment period for signs of morbidity and mortality. Tumor length and width as well as animal weights were measured twice weekly. Tumor volume was calculated using the empirical formula $V = \text{length} \times \text{width}^2 \times 0.52$. The percentage change in each tumor volume was calculated using the formula $((V2 - V1)/V1) \times 100$, where $V1$ is the starting tumor volume and $V2$ is the final tumor volume.

Preparation of Whole-Cell Extracts and Western Blotting

Cells were lysed in 1× RIPA lysis buffer supplemented with phosphatase and protease inhibitors. The whole-cell extracts were then denatured in 2× Laemmli sample buffer at 55°C for 15 minutes, resolved on 4% to 12% NuPAGE gels (Invitrogen), and transferred onto polyvinylidene fluoride (PVDF) membranes. Membranes were blocked in 3% BSA in tris-buffered saline supplemented with 0.1% Tween-20 (vol/vol) for 1 hour at room temperature and probed with primary antibodies (see Supplementary Table S2 for a complete list of antibodies and specificity). Bound antibodies were detected with peroxidase-labeled goat secondary antibody raised against mouse or rabbit IgG (R&D Systems) and imaged with enhanced chemiluminescence (ECL) Western blotting detection reagent (GE Healthcare). Images were captured on X-ray films. Western blotting was conducted at least two times from independently prepared samples.

Proteome Profiling Arrays

We used a human proteome profiling array system (R&D Systems) that contains duplicate validated positive and negative controls and captures antibodies that can simultaneously detect the phosphorylation state of 43 human kinases (Proteome Profiler Human Phospho-Kinase Array Kit; for coordinate annotation, see https://www.rndsystems.com/; ref. 31). Five million cells were plated in 10-cm dishes and grown for 48 hours. Cells were deprived of serum by culturing for 24 hours in growth media supplemented with 0.05% FBS. Whole-cell extracts were then prepared, and detection of protein phosphorylation was carried out according to the manufacturer's

instructions. In brief, the array membranes were blocked, incubated with 350 µg total cellular protein per array overnight at 4°C on a rocking platform, washed, and incubated with phospho-specific detection antibodies. Captured phosphorylated proteins were detected by ECL and imaged on X-ray films. The average pixel densities of duplicate spots were measured using ImageJ software and are expressed relative to the positive control on each array.

^{51}Chromium Release Assays

ADCC was assessed using a ^{51}Cr release assay. Briefly, tumor cells were labeled with sodium ^{51}Cr chromate (Amersham) at 100 mCi/10^6 cells at 37°C for 1 hour. After two washes, tumor cells were plated in a 96-well plate before mixing with human peripheral mononuclear cells with various concentrations of Zeno, trastuzumab, or nonspecific IgG1. Cytotoxicity was analyzed after incubation at 37°C for 4 hours. The released ^{51}Cr was measured by a gamma counter (Packed Instrument). Percentage of specific lysis was calculated using the formula: $100\% \times$ (experimental cpm − background cpm)/(total cpm − background cpm), where cpm represent counts per minute of ^{51}Cr released. Total release of ^{51}Cr was assessed by lysis with 10% SDS, and background release was measured in the absence of effector cells and antibodies.

Molecular Diagnostics, Patients, and Treatments

The single-patient protocols were approved by the MSKCC Institutional Review Board. Written informed consent was obtained from patients, and the study was conducted in accordance with the guidelines of the Declaration of Helsinki. All patient samples were profiled using our center's MSK-IMPACT platform, which is a large-panel NGS assay designed to detect mutations, copy-number alterations, and selected fusions involving up to 505 cancer-associated genes (32). Two patients were also profiled using an RNA-based solid tumor fusion panel assay (MSK-Fusion; ref. 33). Patients with *NRG1* fusion–positive tumors were treated with Zeno (750 mg intravenously, every 2 weeks) on FDA-approved single-patient protocols. Response to therapy was assessed by CT scans using RECIST v1.1 criteria (35).

Statistical Analysis

Tumor data sets were compared by two-way ANOVA with Dunnett or Tukey multiple comparison test to determine significance. $P < 0.05$ was considered a statistically significant difference between two values or data sets. AUC analysis was calculated by the trapezoid rule, and groups were compared using one-way ANOVA with two-tailed Student t test. All statistical analyses were conducted using GraphPad Prism 8 software (RRID: SCR_002798). All experiments consisted of two to six replicates per condition, and data are expressed as mean ± SD or SEM as indicated in figure legends.

Data Availability Statement

Data generated in this study are available upon request from the corresponding authors.

Authors' Disclosures

A.M. Schram reports other support from Merus during the conduct of the study, as well as other support from AstraZeneca, ArQule, BeiGene, Black Diamond Thereapeutics, Elevation Oncology, Kura Oncology, Lilly, Northern Biologics, Pfizer, PMV Pharma, Relay Therapeutics, Repare Therapeutics, Revolution Medicine, and Surface Oncology outside the submitted work. S.H. Shameem reports personal fees from Regeneron Pharmaceuticals outside the submitted work. J. Ford reports other support from Merus N.V. outside the submitted work. M.N. O'Connor is an employee of Merus N.V. C.A. Geuijen reports personal fees from Merus N.V. during the conduct of the study; personal fees from Merus N.V. outside the

submitted work; and patents for Zeno issued. R.C.J. Schackmann reports personal fees from Merus N.V. outside the submitted work. J.J. Lammerts van Bueren reports personal fees from Merus N.V. and other support from Merus N.V. during the conduct of the study, as well as personal fees from Merus N.V. and other support from Merus N.V. outside the submitted work. E. Wasserman reports personal fees from Merus N.V. and other support from Merus N.V. during the conduct of the study. E.M. O'Reilly reports grants from Genentech/Roche, Celgene/Bristol Myers Squibb, BioNTech, AstraZeneca, Arcus, Elicio, Parker Institute, Seagen, Boehringer Ingelheim, BioNTech, Ipsen, Merck, IDEAYA, AstraZeneca, Noxxon, BioSapien, Cend Therapeutics, and Thetis and other support from CytomX Therapeutics, Rafael Therapeutics, Agios, Genentech/Roche, and Eisai during the conduct of the study. M. Ladanyi reports grants from Merus during the conduct of the study, as well as grants from Elevation Oncology and nonfinancial support from Glaxo-SmithKline outside the submitted work. A. Drilon reports personal fees from Ignyta/Genentech/Roche, Loxo/Bayer/Lilly, Takeda/Ariad/Millenium, TP Therapeutics, AstraZeneca, Pfizer, Blueprint Medicines, Helsinn, Beigene, BerGenBio, Hengrui Therapeutics, Exelixis, Tyra Biosciences, Verastem, MORE Health, AbbVie, 14ner/Elevation Oncology, ArcherDX, Monopteros, Novartis, EMD Serono, Medendi, Repare RX, Nuvalent, Merus, Chugai Pharmaceutical, Remedica Ltd., mBrace, AXIS, EPG Health, Harborside Nexus, Liberum, RV More, Ology, Amgen, TouchIME, Janssen, Entos, Treeline Bio, Prelude, and Applied Pharmaceutical Science, Inc. during the conduct of the study; other support from Pfizer, Exelixis, GlaxoSmithKline, Teva, Taiho, and PharmaMar outside the submitted work; a patent for selpercatinib and osimertinib pending; royalties from Wolters Kluwer; other (food/beverage) from Merck, Puma, Merus, and Boehringer Ingelheim; and CME honoraria from Medscape, OncLive, PeerVoice, Physicians Education Resources, Targeted Oncology, Research to Practice, Axis, Peerview Institute, Paradigm Medical Communications, WebMD, MJH Life Sciences, AXIS, EPG Health, and JNCC/Harborside. R. Somwar reports grants and nonfinancial support from Merus during the conduct of the study, as well as grants and nonfinancial support from Elevation Oncology, Helsinn Health Care, and Loxo Oncology and nonfinancial support from GlaxoSmithKline outside the submitted work. No disclosures were reported by the other authors.

Authors' Contributions

A.M. Schram: Conceptualization, resources, data curation, formal analysis, supervision, funding acquisition, validation, investigation, visualization, methodology, writing–original draft, writing–review and editing. **I. Odintsov:** Conceptualization, resources, data curation, formal analysis, validation, investigation, visualization, methodology, writing–original draft, writing–review and editing. **M. Espinosa-Cotton:** Formal analysis, investigation, writing–review and editing. **I. Khodos:** Resources, investigation, methodology, writing–review and editing. **W.J. Sisso:** Resources, investigation, methodology, writing–review and editing. **M.S. Mattar:** Resources, supervision, investigation, methodology, writing–review and editing. **A.J.W. Lui:** Resources, investigation, writing–review and editing. **M. Vojnic:** Data curation, investigation, writing–review and editing. **S.H. Shameem:** Investigation, methodology, writing–review and editing. **T. Chauhan:** Conceptualization, resources, methodology, writing–review and editing. **J. Torrisi:** Data curation, formal analysis, investigation, writing–review and editing. **J. Ford:** Resources, methodology, writing–review and editing. **M.N. O'Connor:** Resources, investigation. **C.A.W. Geuijen:** Conceptualization, resources, data curation, investigation, methodology, writing–review and editing. **R.C.J. Schackmann:** Conceptualization, resources, data curation, supervision, investigation, methodology, writing–review and editing. **J.J. Lammerts van Bueren:** Conceptualization, funding acquisition, methodology, writing–review and editing. **E. Wasserman:** Resources,

REFERENCES

1. Jonna S, Feldman RA, Swensen J, Gatalica Z, Korn WM, Borghaei H, et al. Detection of NRG1 gene fusions in solid tumors. Clin Cancer Res 2019;25:4966–72.
2. Ptakova N, Martinek P, Holubec L, Janovsky V, Vancurova J, Grossmann P, et al. Identification of tumors with NRG1 rearrangement, including a novel putative pathogenic UNC5D-NRG1 gene fusion in prostate cancer by data-drilling a de-identified tumor database. Genes Chromosomes Cancer 2021;60:474–81.
3. Huang HE, Chin SF, Ginestier C, Bardou VJ, Adelaide J, Iyer NG, et al. A recurrent chromosome breakpoint in breast cancer at the NRG1/neuregulin 1/heregulin gene. Cancer Res 2004;64:6840–4.
4. Fernandez-Cuesta L, Plenker D, Osada H, Sun R, Menon R, Leenders F, et al. CD74-NRG1 fusions in lung adenocarcinoma. Cancer Discov 2014;4:415–22.
5. Dhanasekaran SM, Balbin OA, Chen G, Nadal E, Kalyana-Sundaram S, Pan J, et al. Transcriptome meta-analysis of lung cancer reveals recurrent aberrations in NRG1 and Hippo pathway genes. Nat Commun 2014;5:5893.
6. Nakaoku T, Tsuta K, Ichikawa H, Shiraishi K, Sakamoto H, Enari M, et al. Druggable oncogene fusions in invasive mucinous lung adenocarcinoma. Clin Cancer Res 2014;20:3087–93.
7. Heining C, Horak P, Uhrig S, Codo PL, Klink B, Hutter B, et al. NRG1 fusions in KRAS wild-type pancreatic cancer. Cancer Discov 2018;8:1087–95.
8. Jones MR, Williamson LM, Topham JT, Lee MKC, Goytain A, Ho J, et al. NRG1 gene fusions are recurrent, clinically actionable gene rearrangements in KRAS wild-type pancreatic ductal adenocarcinoma. Clin Cancer Res 2019;25:4674–81.
9. Chang JC, Offin M, Falcon C, Brown D, Houck-Loomis BR, Meng F, et al. Comprehensive molecular and clinicopathologic analysis of 200 pulmonary invasive mucinous adenocarcinomas identifies distinct characteristics of molecular subtypes. Clin Cancer Res 2021;27:4066–76.
10. Laskin J, Liu SV, Tolba K, Heining C, Schlenk RF, Cheema P, et al. NRG1 fusion-driven tumors: biology, detection, and the therapeutic role of afatinib and other ErbB-targeting agents. Ann Oncol 2020;31:1693–703.
11. Bernardino J, Apiou F, Gerbault-Seureau M, Malfoy B, Dutrillaux B. Characterization of recurrent homogeneously staining regions in 72 breast carcinomas. Genes Chromosomes Cancer 1998;23:100–8.
12. Wang XZ, Jolicoeur EM, Conte N, Chaffanet M, Zhang Y, Mozziconacci MJ, et al. Gamma-heregulin is the product of a chromosomal translocation fusing the DOC4 and HGL/NRG1 genes in the MDA-MB-175 breast cancer cell line. Oncogene 1999;18:5718–21.
13. Liu X, Baker E, Eyre HJ, Sutherland GR, Zhou M. Gamma-heregulin: a fusion gene of DOC-4 and neuregulin-1 derived from a chromosome translocation. Oncogene 1999;18:7110–4.
14. Shin DH, Lee D, Hong DW, Hong SH, Hwang JA, Lee BI, et al. Oncogenic function and clinical implications of SLC3A2-NRG1 fusion in invasive mucinous adenocarcinoma of the lung. Oncotarget 2016;7:69450–65.
15. Weinstein EJ, Leder P. The extracellular region of heregulin is sufficient to promote mammary gland proliferation and tumorigenesis but not apoptosis. Cancer Res 2000;60:3856–61.
16. Roskoski R Jr. The ErbB/HER receptor protein-tyrosine kinases and cancer. Biochem Biophys Res Commun 2004;319:1–11.
17. Wang Z. ErbB receptors and cancer. Methods Mol Biol 2017;1652:3–35.
18. Tzahar E, Levkowitz G, Karunagaran D, Yi L, Peles E, Lavi S, et al. ErbB-3 and ErbB-4 function as the respective low and high affinity receptors of all Neu differentiation factor/heregulin isoforms. J Biol Chem 1994;269:25226–33.
19. Yarden Y, Sliwkowski MX. Untangling the ErbB signalling network. Nat Rev Mol Cell Biol 2001;2:127–37.
20. Zhang X, Gureasko J, Shen K, Cole PA, Kuriyan J. An allosteric mechanism for activation of the kinase domain of epidermal growth factor receptor. Cell 2006;125:1137–49.
21. van Lengerich B, Agnew C, Puchner EM, Huang B, Jura N. EGF and NRG induce phosphorylation of HER3/ERBB3 by EGFR using distinct oligomeric mechanisms. Proc Natl Acad Sci U S A 2017;114:E2836–E45.
22. Chen CH, Chernis GA, Hoang VQ, Landgraf R. Inhibition of heregulin signaling by an aptamer that preferentially binds to the oligomeric form of human epidermal growth factor receptor-3. Proc Natl Acad Sci U S A 2003;100:9226–31.
23. Klapper LN, Glathe S, Vaisman N, Hynes NE, Andrews GC, Sela M, et al. The ErbB-2/HER2 oncoprotein of human carcinomas may function solely as a shared coreceptor for multiple stroma-derived growth factors. Proc Natl Acad Sci U S A 1999;96:4995–5000.
24. Drilon A, Somwar R, Mangatt BP, Edgren H, Desmeules P, Ruusulehto A, et al. Response to ERBB3-directed targeted therapy in NRG1-rearranged cancers. Cancer Discov 2018;8:686–95.
25. Cadranel J, Liu SV, Duruisseaux M, Branden E, Goto Y, Weinberg BA, et al. Therapeutic potential of afatinib in NRG1 fusion-driven solid tumors: a case series. Oncologist 2021;26:7–16.
26. Geuijen CAW, De Nardis C, Maussang D, Rovers E, Gallenne T, Hendriks LJA, et al. Unbiased combinatorial screening identifies a bispecific IgG1 that potently inhibits HER3 signaling via HER2-guided ligand blockade. Cancer Cell 2018;33:922–36.
27. Odintsov I, Lui AJW, Sisso WJ, Gladstone E, Liu Z, Delasos L, et al. The anti-HER3 mAb seribantumab effectively inhibits growth of patient-derived and isogenic cell line and xenograft models with oncogenic NRG1 fusions. Clin Cancer Res 2021;27:3154–66.
28. Alsina M, Boni V, Schellens JHM, Moreon V, Bol K, Westendorp M, et al. First-in-human phase 1/2 study of MCLA-128, a full length IgG1 bispecific antibody targeting HER2 and HER3: final phase 1 data and preliminary activity in HER2+ metastatic breast cancer (MBC). J Clin Oncol 35, 2017 (suppl; abstr 2522).
29. Odintsov I, Mattar MS, Lui AJW, Offin M, Kurzatkowski C, Delasos L, et al. Novel preclinical patient-derived lung cancer models reveal inhibition of HER3 and MTOR signaling as therapeutic strategies for NRG1 fusion-positive cancers. J Thorac Oncol 2021;16:1149–65.
30. Howarth KD, Mirza T, Cooke SL, Chin SF, Pole JC, Turro E, et al. NRG1 fusions in breast cancer. Breast Cancer Res 2021;23:3.
31. Hayashi T, Odintsov I, Smith RS, Ishizawa K, Liu AJW, Delasos L, et al. RET inhibition in novel patient-derived models of RET-fusion positive lung adenocarcinoma reveals a role for MYC upregulation. Dis Model Mech 2020;14:dmm047779.
32. Cheng DT, Mitchell TN, Zehir A, Shah RH, Benayed R, Syed A, et al. Memorial Sloan Kettering-Integrated Mutation Profiling of Actionable Cancer Targets (MSK-IMPACT): a hybridization capture-

based next-generation sequencing clinical assay for solid tumor molecular oncology. J Mol Diagn 2015;17:251–64.

33. Benayed R, Offin M, Mullaney K, Sukhadia P, Rios K, Desmeules P, et al. High yield of RNA sequencing for targetable kinase fusions in lung adenocarcinomas with no mitogenic driver alteration detected by DNA sequencing and low tumor mutation burden. Clin Cancer Res 2019;25:4712–22.

34. Ulaner GA, Saura C, Piha-Paul SA, Mayer I, Quinn D, Jhaveri K, et al. Impact of FDG PET imaging for expanding patient eligibility and measuring treatment response in a genome-driven basket trial of the Pan-HER kinase inhibitor, neratinib. Clin Cancer Res 2019;25:7381–7.

35. Eisenhauer EA, Therasse P, Bogaerts J, Schwartz LH, Sargent D, Ford R, et al. New response evaluation criteria in solid tumours: revised RECIST guideline (version 1.1). Eur J Cancer 2009;45:228–47.

36. Brannon AR, Jayakumaran G, Diosdado M, Patel J, Razumova A, Hu Y, et al. Enhanced specificity of clinical high-sensitivity tumor mutation profiling in cell-free DNA via paired normal sequencing using MSK-ACCESS. Nat Commun 2021;12:3770.

37. Conroy T, Desseigne F, Ychou M, Bouche O, Guimbaud R, Becouarn Y, et al. FOLFIRINOX versus gemcitabine for metastatic pancreatic cancer. N Engl J Med 2011;364:1817–25.

38. Moore MJ, Goldstein D, Hamm J, Figer A, Hecht JR, Gallinger S, et al. Erlotinib plus gemcitabine compared with gemcitabine alone in patients with advanced pancreatic cancer: a phase III trial of the National Cancer Institute of Canada Clinical Trials Group. J Clin Oncol 2007;25:1960–6.

39. Kindler HL, Niedzwiecki D, Hollis D, Sutherland S, Schrag D, Hurwitz H, et al. Gemcitabine plus bevacizumab compared with gemcitabine plus placebo in patients with advanced pancreatic cancer: phase III trial of the Cancer and Leukemia Group B (CALGB 80303). J Clin Oncol 2010;28:3617–22.

40. Golan T, Hammel P, Reni M, Van Cutsem E, Macarulla T, Hall MJ, et al. Maintenance olaparib for germline BRCA-mutated metastatic pancreatic cancer. N Engl J Med 2019;381:317–27.

41. Schram A, O'Reilly E, Somwar R, Benayed R, Shameem S, Chauhan T, et al. Clinical proof of concept for MCLA-128, a bispecific HER2/3 antibody therapy, in NRG1 fusion-positive cancers [abstract]. In: Proceedings of the AACR-NCI-EORTC International Conference on Molecular Targets and Cancer Therapeutics; 2019 Oct 26–30; Boston, MA. Philadelphia (PA): AACR; Mol Cancer Ther 2019;18(12 Suppl): Abstract nr PR02.

42. Sequist LV, Yang JC, Yamamoto N, O'Byrne K, Hirsh V, Mok T, et al. Phase III study of afatinib or cisplatin plus pemetrexed in patients with metastatic lung adenocarcinoma with EGFR mutations. J Clin Oncol 2013;31:3327–34.

43. Gan HK, Millward M, Jalving M, Garrido-Laguna I, Lickliter JD, Schellens JHM, et al. A phase I, first-in-human study of GSK2849330, an anti-HER3 monoclonal antibody, in HER3-expressing solid tumors. Oncologist 2021;26:e1844–e53.

44. Soule HD, Vazquez J, Long A, Albert S, Brennan M. A human cell line from a pleural effusion derived from a breast carcinoma. J Natl Cancer Inst 1973;51:1409–16.

45. Corsello SM, Bittker JA, Liu Z, Gould J, McCarren P, Hirschman JE, et al. The Drug Repurposing Hub: a next-generation drug library and information resource. Nat Med 2017;23:405–8.

46. Sato M, Vaughan MB, Girard L, Peyton M, Lee W, Shames DS, et al. Multiple oncogenic changes (K-RAS(V12), p53 knockdown, mutant EGFRs, p16 bypass, telomerase) are not sufficient to confer a full malignant phenotype on human bronchial epithelial cells. Cancer Res 2006;66:2116–28.

47. Li GG, Somwar R, Joseph J, Smith RS, Hayashi T, Martin L, et al. Antitumor activity of RXDX-105 in multiple cancer types with RET rearrangements or mutations. Clin Cancer Res 2017;23:2981–90.

48. Furukawa T, Duguid WP, Rosenberg L, Viallet J, Galloway DA, Tsao MS. Long-term culture and immortalization of epithelial cells from normal adult human pancreatic ducts transfected by the E6E7 gene of human papilloma virus 16. Am J Pathol 1996;148: 1763–70.